Accelerated Late Gadolinium Enhancement Cardiac MR Imaging with Isotropic Spatial Resolution Using Compressed Sensing: Initial Experience[1]

Mehmet Akçakaya, PhD
Hussein Rayatzadeh, MD
Tamer A. Basha, PhD
Susie N. Hong, MD
Raymond H. Chan, MD
Kraig V. Kissinger, RT, MS
Thomas H. Hauser, MD
Mark E. Josephson, MD
Warren J. Manning, MD
Reza Nezafat, PhD

Purpose: To evaluate the use of low-dimensional-structure self-learning and thresholding (LOST) compressed sensing acquisition and reconstruction in the assessment of left atrial (LA) and left ventricular (LV) scar by using late gadolinium enhancement (LGE) magnetic resonance (MR) imaging with isotropic spatial resolution.

Materials and Methods: The study was approved by the local institutional review board and was compliant with HIPAA. All subjects provided written informed consent. Twenty-eight patients (eight women; mean age, 58.0 years ± 10.1) with a history of atrial fibrillation were recruited for the LA LGE study, and 14 patients (five women; mean age, 54.2 years ± 18.6) were recruited for assessment of LV myocardial infarction. With use of a pseudorandom k-space undersampling pattern, threefold accelerated three-dimensional (3D) LGE data were acquired with isotropic spatial resolution and reconstructed off-line by using LOST. For comparison, subjects were also imaged by using standard 3D LGE protocols with nonisotropic spatial resolution. Images were compared qualitatively by three cardiologists with regard to diagnostic value, presence of enhancement, and image quality. The signed rank test and Wilcoxon unpaired two-sample test were used to test the hypothesis that there would be no significant difference in image quality ratings with different resolutions.

Results: Interpretable images were obtained in 26 of the 28 patients (93%) in the LA LGE study. LGE was seen in 17 of 30 cases (57%) with nonisotropic resolution and in 18 cases (60%) with isotropic resolution. Diagnostic quality scores of isotropic images were significantly higher than those of nonisotropic images with coronal views (median, 3 vs 2, respectively [25th and 75th percentiles: 3, 3 vs 2, 3]; $P < .001$) and sagittal views (median, 3 vs 2 [25th and 75th percentiles: 3, 4 vs 2, 3]; $P < .001$) but lower with axial views (median, 4 vs 3 [25th and 75th percentiles: 3, 4 vs 3, 3]; $P < .001$). For the LV LGE study, all patients had interpretable images. LGE was seen in six of 14 patients (43%), with 100% agreement between both data sets. Diagnostic quality scores of high-isotropic-resolution LV images were higher than those of nonisotropic images with short-axis views (median, 4 vs 3 [25th and 75th percentiles: 3, 4 vs 2, 3]; $P = .014$) and two-chamber views (median, 4 vs 3 [25th and 75th percentiles: 3, 4 vs 2, 3]; $P = .001$).

Conclusion: An accelerated LGE acquisition with LOST enables imaging with high isotropic spatial resolution for improved assessment of LV, LA, and pulmonary vein scar.

Supplemental material: *http://radiology.rsna.org/lookup/suppl/doi:10.1148/radiol.12112489/-/DC1*

[1] From the Departments of Medicine (M.A., H.R., T.A.B., S.N.H., R.H.C., K.V.K., T.H.H., M.E.J., W.J.M., R.N.) and Radiology (W.J.M.), Beth Israel Deaconess Medical Center and Harvard Medical School, 330 Brookline Ave, Boston, MA 02215. Received November 28, 2011; revision requested January 19, 2012; revision received March 5; accepted March 20; final version accepted March 30. **Address correspondence to** R.N. (e-mail: *rnezafat@bidmc.harvard.edu*).

Two-dimensional late gadolinium enhancement (LGE, ie, delayed enhancement) magnetic resonance (MR) imaging (1,2) is the clinical reference standard for the imaging of scar and/or fibrosis in the left ventricle (LV) in both ischemic and nonischemic cardiomyopathy (3–8). Anatomic tissue heterogeneity at LGE MR imaging increases the susceptibility to ventricular arrhythmias in patients with chronic myocardial infarction and LV dysfunction (3). This heterogeneous tissue or "gray zone" (area with intermediate signal intensity at LGE imaging) (3) surrounding or within dense LGE scar has also been shown to be the imaging equivalent of arrhythmogenic zones (3,9–11). This area is also a predictor of all-cause mortality in patients with coronary artery disease (4). However, accurate characterization of this area is dependent on the spatial resolution of the image (12). Beyond the role of LV LGE imaging for the visualization of scar, recent studies demonstrated the utility of LGE imaging for assessing the results of radiofrequency ablation in the left atrium (LA) and pulmonary veins in patients undergoing pulmonary vein isolation for the treatment of atrial fibrillation (13–16). LA LGE imaging can also be used to identify preexisting scars for risk stratification and selection of patients for ablation (15) and to predict the risk of stroke in patients with atrial fibrillation (17). LA LGE imaging demands three-dimensional (3D) LGE acquisition with substantially higher spatial resolution than that for LV LGE imaging to assess the thinner LA and pulmonary vein wall.

The use of 3D acquisition improves the signal-to-noise ratio (SNR) of LGE imaging, thereby facilitating increased spatial resolution. However, 3D imaging substantially prolongs the imaging time, which may deteriorate image quality because the image is more susceptible to variations in heart rate and respiratory motion, temporal changes in the accumulation of the contrast material in the scar area, and changes in the optimal inversion time. Thus, despite their potential to improve the spatial resolution, current 3D LGE techniques are limited by long imaging times that frequently result in nondiagnostic images. Furthermore, a 3D acquisition with high isotropic spatial resolution would enable visualization of the enhancement from any orientation, enabling improved depiction of scar morphology and superior characterization of the heterogeneous zone. However, accelerated imaging is required to achieve a higher spatial resolution and to mitigate artifacts due to changes in inversion time and heart rate variability.

Compressed sensing is a recent technique for rapid imaging with incoherently undersampled k-space data that exploits the compressibility of images in transform domains (18) and may provide faster imaging than current techniques (19). Recently, we proposed an improved compressed sensing–based reconstruction strategy called low-dimensional-structure self-learning and thresholding (LOST) (20). This technique uses patient- and anatomic-specific information from low-spatial-resolution images reconstructed from the fully sampled central k-space data to adaptively generate a sparse representation for the undersampled image. This reconstruction reduces blurring artifacts associated with conventional compressed sensing reconstruction for high-spatial-resolution cardiac MR imaging (20).

We performed this study to evaluate the use of LOST compressed sensing acquisition and reconstruction in the assessment of LA and LV scar by using LGE MR imaging with isotropic spatial resolution.

Advances in Knowledge

- Low-dimensional-structure self-learning and thresholding (LOST) allows acquisition of late gadolinium enhancement (LGE) MR images with high isotropic spatial resolution.
- Isotropic-spatial-resolution LGE MR imaging allows detailed visualization of left ventricular scar morphology.
- LGE MR imaging of pulmonary veins with isotropic resolution allows improved multiplanar assessment of scar in the pulmonary veins and left atrium.

Implications for Patient Care

- Three-dimensional high-spatial-resolution LGE MR imaging can be used in both patients with and patients without ischemia for improved visualization of scar characteristics.
- Isotropic LGE MR imaging of the left atrium can depict the extent of scar after ablation and may be used to better assess for noncardiac damage in structures such as the esophagus.

Materials and Methods

All MR sequences were implemented with a 1.5-T unit (Achieva; Philips Healthcare, Best, the Netherlands) with a five-channel cardiac phased-array receiver coil. Our study complied with the Health Insurance Portability and Accountability Act and was approved by our institutional

Published online before print
10.1148/radiol.12112489 **Content code:** CA

Radiology 2012; 264:691–699

Abbreviations:
LA = left atrium
LGE = late gadolinium enhancement
LOST = low-dimensional-structure self-learning and thresholding
LV = left ventricle
SNR = signal-to-noise ratio
3D = three-dimensional

Author contributions:
Guarantors of integrity of entire study, M.A., M.E.J., R.N.; study concepts/study design or data acquisition or data analysis/interpretation, all authors; manuscript drafting or manuscript revision for important intellectual content, all authors; approval of final version of submitted manuscript, all authors; literature research, M.A., H.R., R.H.C., M.E.J., R.N.; clinical studies, M.A., H.R., S.N.H., K.V.K., T.H.H., M.E.J., W.J.M., R.N.; statistical analysis, M.A., R.H.C., T.H.H.; and manuscript editing, M.A., H.R., S.N.H., R.H.C., K.V.K., T.H.H., M.E.J., W.J.M., R.N.

Funding:
This research was supported by the National Institutes of Health (grants R01EB008743-01A2 and UL1 RR025758-01).

Potential conflicts of interest are listed at the end of this article.

review board. Written informed consent was obtained from all participants.

Accelerated Image Acquisition

A 3D randomly undersampled acquisition sequence was implemented for the accelerated acquisitions, and a net acceleration rate of 3.0 in k_y-k_z was used. For each acquisition, a pseudorandom k-space undersampling pattern that fully sampled the central k-space (of size 45 × 35 in k_y-k_z), and randomly discarded the edges, was generated. This undersampling pattern was then stored as a look-up table. Because the profile ordering in which these lines were acquired has an effect on image contrast, and because rapid gradient switching may lead to eddy current and flow artifacts, a profile reordering was performed before the acquisition. The selected k_y-k_z lines were sorted on the basis of their k_y and k_z location in a radial fashion (21), which was used to reduce gradient switching by limiting the jumps in k-space between consecutively acquired lines while acquiring the desired random undersampling pattern.

Image Reconstruction

We have previously reported the details of LOST reconstruction and comparison with conventional compressed sensing methods (20). Briefly, the LOST reconstruction adaptively finds a sparse representation for a given image by using the structure and anatomic features in the image being reconstructed instead of relying on a predetermined fixed transform domain (eg, wavelet transforms). An estimate of the image is used to adaptively identify two-dimensional image blocks of similar signal content, which are grouped into similarity clusters. For each voxel of the image, the reference block whose top left corner is at that voxel is compared by using the normalized Euclidean distance to another block. If this distance is less than a threshold, these blocks are declared similar and the compared block is added to the similarity cluster of that voxel. Then, a 3D fast Fourier transform is applied to each similarity cluster to adaptively sparsify the data (20). The algorithm then alternates between data consistency and shrinkage of the 3D fast Fourier transform coefficients of the similarity clusters. The implementation details are provided in Appendix E1 (online).

LOST reconstruction was implemented in Matlab (v7.9; MathWorks, Natick, Mass), with the adaptive learning and nonlinear shrinkage portions implemented in C++, and performed off-line for each coil independently by using a parallel implementation on a central processing unit cluster. Final images were generated by using the root-sum-of-squares method on the individual coil images.

Patient Study

In a prospective study of LA LGE, 28 patients with a history of atrial fibrillation (20 men, eight women; mean age ± standard deviation, 58.0 years ± 10.1) were recruited. Imaging was performed before pulmonary vein isolation in 15 patients (nine men, six women; mean age, 62.4 years ± 10.5), including two with a history of remote pulmonary vein isolation, after pulmonary vein isolation in 10 (eight men, two women; mean age, 57.7 years ± 6.4), and both before and after pulmonary vein isolation in three (men; mean age, 47.3 years ± 6.5), including one patient with a history of ablation, for a total of 31 cases. For LV LGE imaging, 14 patients (nine men, five women; mean age, 54.2 years ± 18.6) referred for evaluation of myocardial infarction were recruited. Patients were excluded if they had a contraindication to MR imaging. All subjects were in sinus rhythm during MR imaging acquisitions.

LGE images were acquired 10–20 minutes after infusion of a bolus (2 mL/sec) of 0.2 mmol/kg gadopentetate dimeglumine (Magnevist; Bayer Schering Pharma, Berlin, Germany) or 0.1–0.2 mmol/kg gadobenate dimeglumine (MultiHance; Bracco, Rome, Italy). All patients with an estimated glomerular filtration rate of less than 60 mL/min/1.73 m^2 received 0.1 mmol/kg gadobenate dimeglumine. The optimal inversion time was selected to null the LV myocardial signal by using a Look-Locker sequence before each LGE image. A free-breathing electrocardiography-triggered navigator-gated inversion-recovery gradient-echo sequence was used for all acquisitions. Imaging parameters were as follows: repetition time of 5.2 msec, echo time of 2.6 msec (5.2/2.6), field of view of 320 × 400 × 90 mm^3 for LA LGE imaging and 320 × 320 × 120 mm^3 for LV LGE imaging, and flip angle of 25°. A respiratory navigator (two-dimensional spiral pencil beam) placed on the dome of the right hemidiaphragm was used for respiratory motion compensation with use of prospective real-time correction with a 5-mm end-expiration gating window (22,23). Saturation bands along the phase-encoding direction were used to reduce fold-over artifacts. A right-left phase-encoding direction was used to reduce respiratory artifacts from the chest wall.

For each patient, images were obtained with a standard nonisotropic 3D LGE sequence and a threefold LOST-accelerated high-isotropic-resolution 3D LGE sequence. Image acquisitions were performed axially, except for two nonisotropic LV LGE acquisitions, which were prescribed in the LV short axis. The order of these images was randomized to cancel out differences due to acquisition time after contrast material injection. The spatial resolution of the standard nonisotropic 3D LGE image was 1.7 × 1.7 × 4.0 mm^3 for LV LGE imaging and 1.4 × 1.4 × 4.0 mm^3 for LA LGE imaging. The spatial resolution of isotropic images was 1.4 × 1.4 × 1.4 mm^3 for LA LGE imaging and varied from 1.2 × 1.2 × 1.2 mm^3 to 1.7 × 1.7 × 1.7 mm^3 for LV LGE imaging. The total acquisition times were approximately 4 minutes for LA LGE imaging and approximately 3 minutes for LV LGE imaging (with 1.7-mm in-plane spatial resolution) at a heart rate of 70 beats per minute and 100% navigator efficiency for both nonisotropic and LOST-accelerated isotropic images.

Image and Statistical Analysis

Reconstructed LGE images were written into Digital Imaging and Communications in Medicine format and imported into a ViewForum workstation (model vR4.2V1L2, Philips Healthcare) for analysis. A subjective qualitative

Figure 1

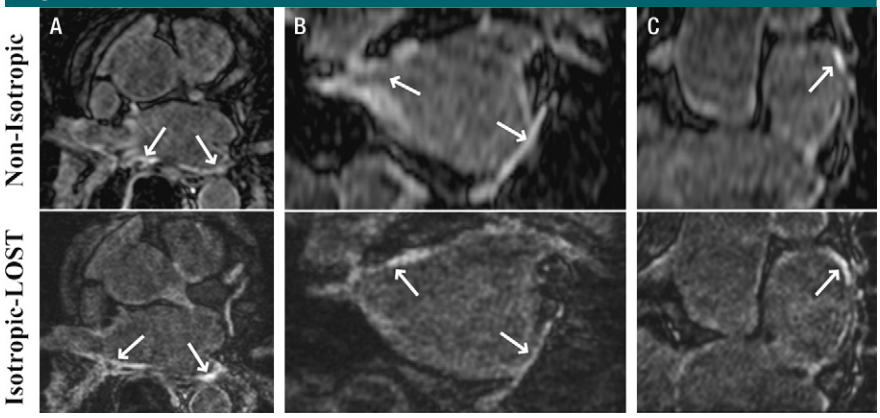

Figure 1: *A*, Axial, *B*, coronal, and, *C*, multiplanar reformatted 3D LA LGE MR images (5.2/2.6; section thickness, 4 mm [nonisotropic] and 1.4 mm [isotropic]; matrix, 456 × 256; field of view, 320 × 400 cm^2) obtained with nonisotropic and isotropic resolution in 54-year-old man who underwent pulmonary vein isolation. Compared with standard nonisotropic images, isotropic resolution images reconstructed with LOST and an acceleration rate of 3.0 enable better visualization at different orientations. Nonisotropic LGE images are degraded by blurring on sagittal and coronal views. Arrows = LA enhancement associated with radiofrequency ablation.

assessment of image quality was performed by consensus of three independent cardiologists (R.H.C., S.N.H., and T.H.H., with 3, 5, and 10 years of experience with cardiac MR imaging, respectively) who were blinded to patient information and history and acquisition scheme. Both original and multiplanar reformatted images were used for subjective assessment. For each data set, diagnostic quality and presence of LGE were assessed by using a dichotomous yes or no question. Furthermore, overall image quality in the assessment of viability and/or scar was evaluated by using a four-point scale, as follows: 1 = poor, 2 = fair, 3 = good, and 4 = excellent. Separate scores were given for different orientations. Original axial, reformatted coronal, and sagittal views were used for LA LGE analysis, and original axial and reformatted short-axis, two-chamber, and four-chamber views were used for LV LGE analysis. The nonisotropic LV LGE analysis was performed with two-dimensional breath-hold imaging for three of the 14 patients and with phase-sensitive inversion recovery (24) for four patients. These data sets were excluded from scoring and further analysis. Imaging scores are presented as medians and 25th and 75th percentiles. For LA LGE analysis, the signed rank test was used for imaging scores to test for the null hypothesis that the central tendency of the difference was zero between the two images with different resolution. Owing to the exclusion of certain nonisotropic data sets in LV LGE analysis, the Wilcoxon unpaired two-sample test was used to test the hypothesis that there will be no significant difference in ratings for image quality between the two images. All statistical analyses were performed by using software (v9.2, SAS Institute, Cary, NC). $P < .05$ was considered indicative of a statistically significant difference.

Results

LA LGE Imaging

LA LGE imaging was completed in all 31 cases. Two data sets (one nonisotropic and one isotropic, in different patients) were declared uninterpretable owing to contrast material washout and imperfect inversion time. These patients were excluded from further paired analysis. LGE was seen in 17 of the remaining 30 cases (57%) on standard LGE images and 18 of the 30 cases (60%) with LOST reconstruction (discrepancy on the patient whose standard LGE image was nondiagnostic).

Figures 1–3 depict representative cases from patients who underwent pulmonary vein isolation. Figure 1 shows axial, coronal, and reformatted images obtained in a 54-year-old patient. Unlike nonisotropic images, isotropic-resolution images reconstructed with LOST can be reformatted into other orientations without causing blurring artifacts. Figure 2 is a sagittal LGE image obtained after pulmonary vein isolation and shows enhancement of the LA and descending aorta. The isotropic resolution of the LOST-reconstructed images allows visualization of separate regions of enhancement, whereas the nonisotropic resolution exhibits blurring of these regions. Reformatted images in a 50-year-old patient are shown in Figure 3. Enhancement in the right and left inferior pulmonary veins is visible with both acquisitions. The advantage of the superior isotropic resolution is evident on the reformatted images, which show the ablation ring on the right inferior pulmonary vein (Fig 3, *B*).

The subjective image scores for LA LGE imaging are shown in Table 1. Isotropic images were scored higher than nonisotropic images in reformatted coronal views (median, 3 vs 2, respectively [25th and 75th percentiles: 3, 3 vs 2, 3]; $P < .001$, signed rank test) and sagittal views (median, 3 vs 2 [25th and 75th percentiles: 3, 4 vs 2, 3]; $P < .001$, signed rank test). However, they were scored lower in the axial view (median, 4 vs 3 [25th and 75th percentiles: 3, 4 vs 3, 3]; $P < .001$, signed rank test).

LV LGE Imaging

LV LGE imaging was completed in all 14 patients. Among the seven nonisotropic acquisitions that were scored, one 3D acquisition was declared uninterpretable. LGE was present in six of the 14 patients (43%) with isotropic acquisition and three of the six patients (50%) with nonisotropic acquisition. There was no discrepancy among patients where both data sets were evaluated.

Figures 4–6 depict representative cases from patients with LGE in the LV. Figure 4 depicts reformatted images from a 46-year-old patient with hypertrophic cardiomyopathy. The standard

nonisotropic images were acquired with a resolution of 1.5 × 1.5 × 4.0 mm^3 with short-axis prescription, and the accelerated images were acquired with isotropic resolution of 1.5 mm with axial prescription. The benefits of the isotropic resolution were apparent on the four-chamber (Fig 4, *B*) and three-chamber (Fig 4, *C*) views, whereas the reformatted images from the nonisotropic image were degraded by blurring artifacts. In Figure 4, *C*, the enhancement in the myocardium on the nonisotropic image was affected by partial volume artifacts, whereas the isotropic image showed two separate regions of enhancement. Figure 5 shows four reformatted images obtained in the same patient from LOST-accelerated isotropic-resolution acquisitions and illustrates the complex geometry of the scar that can be visualized with high-resolution imaging. Examples of LV LGE images obtained in a 32-year-old patient who underwent imaging for evaluation of scar before implantation of an intracardiac defibrillator are shown in Figure 6. Accelerated images were acquired with an isotropic resolution of 1.2 mm, and nonisotropic images were acquired with a resolution of 1.7 × 1.7 × 4.0 mm^3—all with axial prescription. The enhancement in the apex of the heart is visible on the axial images in both cases. The images reformatted to the long axis of the heart are blurred with the nonisotropic resolution; however, the enhancement is clearly visualized on the corresponding isotropic images.

The subjective image scores for LV LGE analysis are shown in Table 2. The high-isotropic-resolution images were scored higher in all of the axial, short-axis, two-chamber, and four-chamber views. The difference was statistically significant for short-axis views (median, 4 vs 3 [25th and 75th percentiles: 3, 4 vs 2, 3]; $P = .014$, Wilcoxon unpaired test) and two-chamber views (median, 4 vs 3 [25th and 75th percentiles: 3, 4 vs 2, 3]; $P = .001$, Wilcoxon unpaired test).

Figure 2

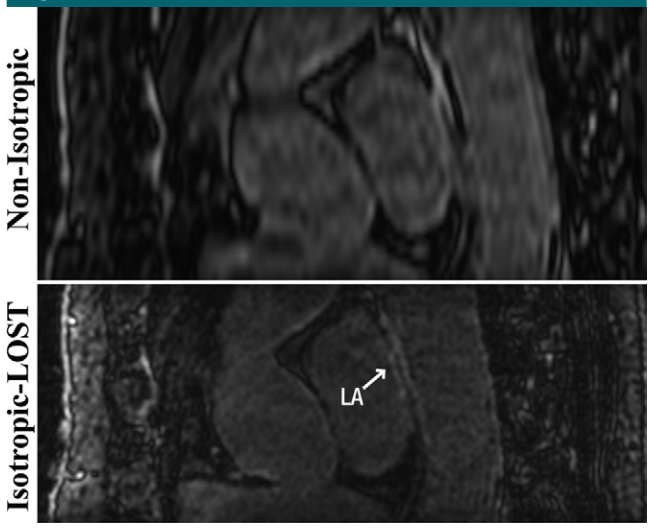

Figure 2: Sagittal 3D LA LGE MR images (5.2/2.6; section thickness, 4 mm [nonisotropic] and 1.4 mm [isotropic]; matrix, 456 × 256; field of view, 320 × 400 cm^2) obtained with nonisotropic and isotropic resolution in 49-year-old woman who underwent pulmonary vein isolation show minor enhancement of LA and descending aorta. Compared with nonisotropic resolution image, LOST-reconstructed isotropic image allows better visualization of separate regions of enhancement; image obtained with nonisotropic resolution exhibits blurring of these regions.

Figure 3

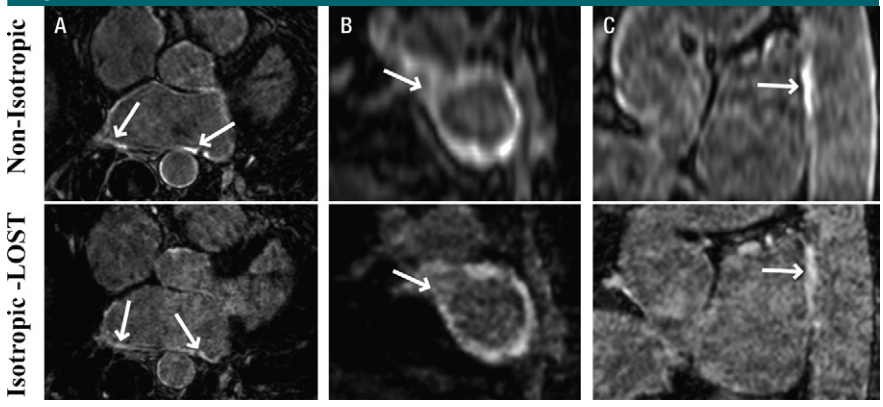

Figure 3: *A*, Axial and, *B*, *C*, reformatted 3D LA LGE MR images (5.2/2.6; section thickness, 4 mm [nonisotropic] and 1.4 mm [isotropic]; matrix, 456 × 256; field of view, 320 × 400 cm^2) obtained with nonisotropic and isotropic resolution in 50-year-old man who underwent pulmonary vein isolation. LOST-reconstructed isotropic images show ablation ring in right inferior pulmonary vein (arrows in *B*) and enhancement in ascending aorta (arrows in *C*), whereas the lower resolution of nonisotropic images hinders clear characterization of enhancement boundaries. Arrows in *A* = enhancement due to ablation.

Discussion

In our study, we demonstrated the feasibility of using 3D LGE imaging with high isotropic spatial resolution (1.2–1.7 mm^3). LOST reconstruction accelerates 3D LGE MR data acquisition by a factor of three by using a clinically available five-channel phased-array cardiac coil system, where the reduced imaging time was traded off for improved isotropic resolution.

The LA wall thickness is approximately 4 mm, and there are substantial

Table 1

LA Analysis: Comparison of Subjective Imaging Scores, Diagnostic Value, and Presence of LGE between Nonisotropic and Accelerated Isotropic Acquisitions

			Median Image Score†		
Technique	Diagnostic Value*	Presence of LGE*	Axial	Coronal	Sagittal
Nonisotropic	30/31 (97)	17/30 (57)	4 (3, 4)	2 (2, 3)	2 (2, 3)
Isotropic LOST	30/31 (97)	18/30 (60)	3 (3, 3)	3 (3, 3)	3 (3, 4)
P value	NA	NA	<.001	<.001	<.001

Note.—Twenty-eight patients underwent LA analysis, and 31 isotropic and nonisotropic images were obtained. Isotropic images reconstructed with LOST were significantly better in coronal and sagittal views, whereas nonisotropic images were significantly better in the axial view (signed rank test). There was no disagreement between the two techniques with regard to the presence of LGE when both acquisitions were diagnostic. Two subject studies were nondiagnostic owing to an incorrect inversion time and contrast material washout.

* Data are numbers of images, with percentages in parentheses. NA = not applicable.

† Image score was reported on a scale of 1 to 4. Numbers in parentheses are the 25th and 75th percentiles, respectively.

Figure 4

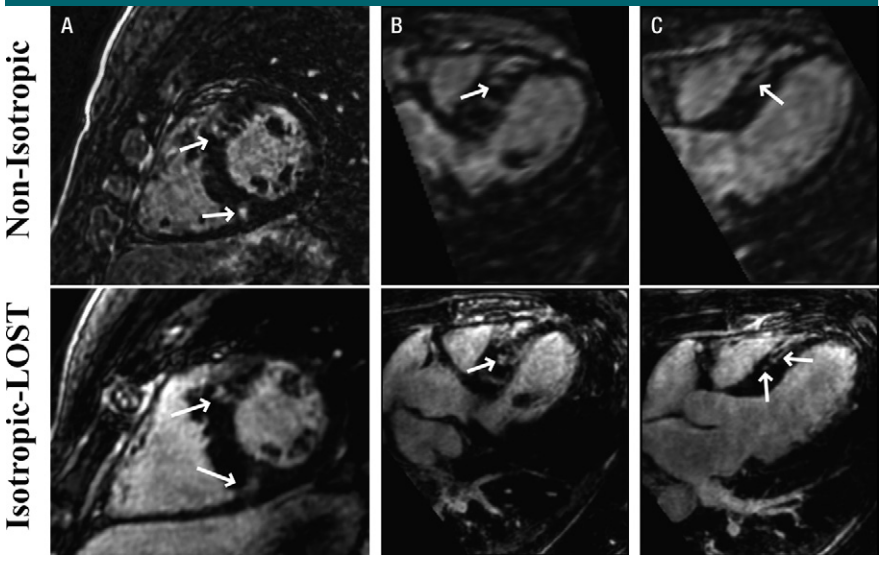

Figure 4: Reformatted 3D LV LGE MR images (5.2/2.6; section thickness, 4 mm [nonisotropic] and 1.5 mm [isotropic]; matrix, 376 × 235; field of view, 320 × 320 cm^2) in, *A*, short-axis, *B*, four-chamber, and, *C*, three-chamber views obtained with nonisotropic and isotropic resolution in 46-year-old man with hypertrophic cardiomyopathy. Isotropic resolution allows superior visualization of scar morphology in three-chamber view (*C*), where two discrete areas of LGE are visualized; only one area of enhancement is seen with nonisotropic imaging. Arrows = regions of enhancement.

interpatient variations in pulmonary vein anatomy and ablation region. Therefore, isotropic resolution imaging is essential to better assess LGE in this region. In addition to the imaging of the LA and pulmonary veins, there have been recent reports of LGE in the esophagus and aorta following pulmonary vein isolation (25–27). Although LA LGE imaging is commonly performed in the axial plane, these anatomic structures are in the foot-head direction and perpendicular to the imaging plane. An isotropic resolution substantially improves visualization in this orientation and provides improved depiction of the 3D anatomic relationships of different structures. For LV LGE imaging, improved resolution will allow superior visualization of the periinfarct zones, which are predictors of mortality and ventricular arrythmia inducibility in patients with coronary artery disease (3,4). In certain cases, the isotropic resolution allows distinction of multiple areas of LGE, which appear as a single area of enhancement on nonisotropic resolution images owing to the lower through-plane resolution.

There is an inherent difference in the SNR between the isotropic and nonisotropic resolution images. Even if the isotropic resolution acquisition were fully sampled, it would have approximately one-third of the SNR of the standard one. Even though the LOST technique inherently thresholds the noise on the reconstructed images, the noise level observed by the cardiologists in our study was still higher than that on nonisotropic images, which affected the subjective image scores in axial view in favor of the nonisotropic images. We note that the accelerated acquisition and nonlinear reconstruction may further reduce the SNR of the final images. However, to our knowledge, SNR quantification for compressed sensing is not yet well understood because these algorithms inherently threshold and shrink the noise in the nonsignal areas, making it difficult to reliably determine the measurement noise from the final reconstructed image. Further studies are needed to better characterize the SNR penalty of such nonlinear reconstruction techniques. In our LV LGE study, imaging with an isotropic spatial resolution of 1.2–1.7 mm^3 was tested to evaluate the feasibility of different spatial resolutions. Our 3D LGE images may have a lower contrast-to-noise ratio owing to the shorter acquisition time and increased noise. However, a decrease in the contrast-to-noise ratio was not reported as a limitation of the image quality by the noninvasive imaging cardiologists who evaluated the images. We also note that because of the randomized acquisition order of the images and the differences in acquisition time after administration of the contrast material, there is an inherent difference in the contrast levels of the two images.

We have not provided a comparison with the clinically available parallel

imaging methods (28–30), although it is not anticipated that these techniques can offer a similar acceleration rate with five-channel coils (15,19). The main difficulty for such a comparison is the conflicting undersampling schemes required by these methods. Although conjugate-gradient type methods can be used with random undersampling in parallel imaging (19,31), these result in performance deterioration and would result in an unfavorable advantage for our method. Because washout of contrast material is an important issue in 3D LGE imaging with imaging times of approximately 10 minutes, it is also not feasible to obtain sequential images with alternate sampling as in our previous study (20). A total imaging time of approximately 30 minutes would be necessary to acquire isotropic resolution images with both undersampling approaches as well as nonisotropic images.

A five-channel coil array was used in our study. The acceleration rates achievable with the proposed technique with use of a 32-channel coil array may be different, but this was not studied. We also note that in previous studies, parallel imaging was only used with a twofold acceleration by using a 32-channel system (15). In addition, although we have used an isotropic resolution of 1.4 mm to assess the LA wall, this resolution may still be insufficient to assess the thin atrial wall. The prognostic value of the improved resolution was also not studied.

In conclusion, a compressed sensing–based LOST acquisition and reconstruction scheme can be used for threefold accelerated LGE MR imaging with high isotropic resolution. Our work is preliminary in showing that compressed sensing–based reconstruction is applicable to LGE imaging for the assessment of LV, LA, and pulmonary vein scar, where the savings in acquisition time can be traded for improved isotropic spatial resolution. Further clinical studies are needed to assess whether the improved spatial resolution will affect diagnostic interpretation of data, including an exploration of the correlation with

Figure 5

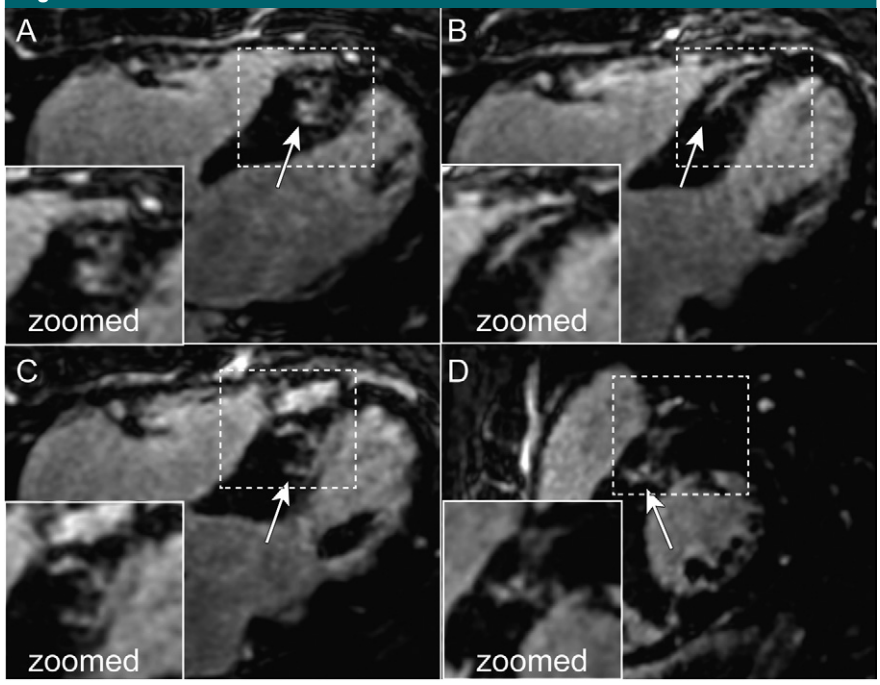

Figure 5: Multiplanar LV reformatted sections from LOST-accelerated 3D LGE MR data set of same patient as in Figure 4 depict details of complex geometry of scar and/or fibrosis, which can be visualized with high isotropic resolution.

Figure 6

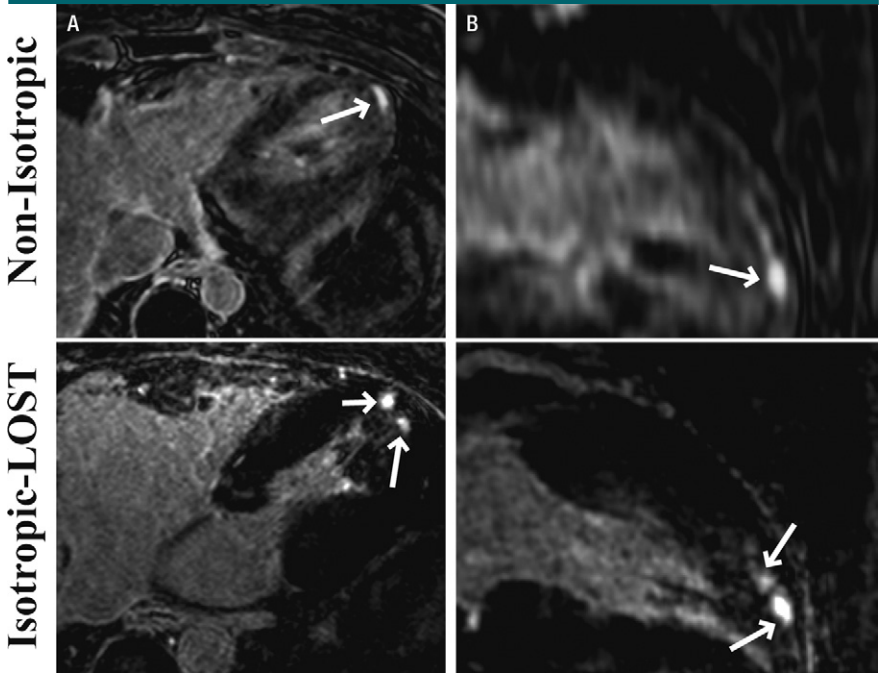

Figure 6: *A*, Axial and, *B*, reformatted long-axis 3D LV LGE MR images (5.2/2.6; section thickness, 4 mm [nonisotropic] and 1.2 mm [isotropic]; matrix, 536 × 319; field of view, 320 × 320 cm^2) obtained with nonisotropic and LOST-accelerated isotropic spatial resolution in 32-year-old man. Scar morphology (arrows) is visualized in greater detail on isotropic LOST images.

Table 2

LV Analysis: Comparison of Subjective Imaging Scores, Diagnostic Value, and Presence of LGE between Nonisotropic and Accelerated Isotropic Acquisitions

			Median Image Score†			
Technique	Diagnostic Value*	Presence of LGE*	Short-Axis View	Two-Chamber View	Four-Chamber View	Axial View
Nonisotropic	6/7 (86)	3/6 (50)	3 (2, 3)	3 (2, 3)	3 (2, 4)	3 (2, 4)
Isotropic LOST	14/14 (100)	6/14 (43)	4 (3, 4)	4 (3, 4)	4 (3, 4)	4 (3, 4)
P value	NA	NA	.014	.001	.271	.271

Note.—Fourteen patients underwent LV evaluation. Nonisotropic LV LGE images were obtained with two-dimensional breath-hold imaging in three patients and with phase-sensitive inversion recovery in four patients; these cases were excluded from scoring and further analysis. Isotropic images reconstructed with LOST were scored higher than nonisotropic images in all views. The differences in short-axis and two-chamber views were statistically significant (Wilcoxon unpaired two-sample test). There was no disagreement about the presence of LGE between the two acquisitions.

* Data are numbers of patients. Numbers in parentheses are percentages. NA = not applicable.

† Image score was reported on a scale of 1 to 4. Numbers in parentheses are 25th and 75th percentiles, respectively.

electroanatomic maps for LA LGE imaging and quantitative comparison of the two images in terms of total infarct and peri-infarct volumes in LV LGE imaging.

Disclosures of Potential Conflicts of Interest: M.A. No potential conflicts of interest to disclose. **H.R**. No potential conflicts of interest to disclose. **T.A.B.** No potential conflicts of interest to disclose. **S.N.H.** No potential conflicts of interest to disclose. **R.H.C.** No potential conflicts of interest to disclose. **K.V.K.** No potential conflicts of interest to disclose. **T.H.H.** Financial activities related to the present article: none to disclose. Financial activities not related to the present article: is a paid consultant for Astellas. Other relationships: none to disclose. **M.E.J.** Financial activities related to the present article: none to disclose. Financial activities not related to the present article: is a paid consultant for Medtronic; institution has grants or grants pending from Medtronic; received payment for lectures including service on speakers bureau from Medtronic and Biotronik; receives payment for development of educational presentations from Medtronic. Other relationships: none to disclose. **W.J.M.** No potential conflicts of interest to disclose. **R.N.** No potential conflicts of interest to disclose.

References

1. Kim RJ, Fieno DS, Parrish TB, et al. Relationship of MRI delayed contrast enhancement to irreversible injury, infarct age, and contractile function. Circulation 1999;100(19):1992–2002.
2. Kim RJ, Wu E, Rafael A, et al. The use of contrast-enhanced magnetic resonance imaging to identify reversible myocardial dysfunction. N Engl J Med 2000;343(20):1445–1453.
3. Schmidt A, Azevedo CF, Cheng A, et al. Infarct tissue heterogeneity by magnetic resonance imaging identifies enhanced cardiac arrhythmia susceptibility in patients with left ventricular dysfunction. Circulation 2007;115(15):2006–2014.
4. Yan AT, Shayne AJ, Brown KA, et al. Characterization of the peri-infarct zone by contrast-enhanced cardiac magnetic resonance imaging is a powerful predictor of post-myocardial infarction mortality. Circulation 2006;114(1):32–39.
5. Roes SD, Borleffs CJ, van der Geest RJ, et al. Infarct tissue heterogeneity assessed with contrast-enhanced MRI predicts spontaneous ventricular arrhythmia in patients with ischemic cardiomyopathy and implantable cardioverter-defibrillator. Circ Cardiovasc Imaging 2009;2(3):183–190.
6. Bello D, Fieno DS, Kim RJ, et al. Infarct morphology identifies patients with substrate for sustained ventricular tachycardia. J Am Coll Cardiol 2005;45(7):1104–1108.
7. Ordovas KG, Higgins CB. Delayed contrast enhancement on MR images of myocardium: past, present, future. Radiology 2011;261(2):358–374.
8. Klem I, Shah DJ, White RD, et al. Prognostic value of routine cardiac magnetic resonance assessment of left ventricular ejection fraction and myocardial damage: an international, multicenter study. Circ Cardiovasc Imaging 2011;4(6):610–619.
9. Halperin HR, Nazarian S. Magnetic resonance identification of the ventricular tachycardia critical isthmus: finding the needle in the haystack. J Am Coll Cardiol 2011;57(2):195–197.
10. Perez-David E, Arenal A, Rubio-Guivernau JL, et al. Noninvasive identification of ventricular tachycardia–related conducting channels using contrast-enhanced magnetic resonance imaging in patients with chronic myocardial infarction: comparison of signal intensity scar mapping and endocardial voltage mapping. J Am Coll Cardiol 2011;57(2):184–194.
11. Estner HL, Zviman MM, Herzka D, et al. The critical isthmus sites of ischemic ventricular tachycardia are in zones of tissue heterogeneity, visualized by magnetic resonance imaging. Heart Rhythm 2011;8(12):1942–1949.
12. Schelbert EB, Hsu LY, Anderson SA, et al. Late gadolinium-enhancement cardiac magnetic resonance identifies postinfarction myocardial fibrosis and the border zone at the near cellular level in ex vivo rat heart. Circ Cardiovasc Imaging 2010;3(6):743–752.
13. Peters DC, Wylie JV, Hauser TH, et al. Detection of pulmonary vein and left atrial scar after catheter ablation with three-dimensional navigator-gated delayed enhancement MR imaging: initial experience. Radiology 2007;243(3):690–695.
14. McGann CJ, Kholmovski EG, Oakes RS, et al. New magnetic resonance imaging–based method for defining the extent of left atrial wall injury after the ablation of atrial fibrillation. J Am Coll Cardiol 2008;52(15):1263–1271.
15. Oakes RS, Badger TJ, Kholmovski EG, et al. Detection and quantification of left atrial structural remodeling with delayed-enhancement magnetic resonance imaging in patients with atrial fibrillation. Circulation 2009;119(13):1758–1767.
16. Peters DC, Wylie JV, Hauser TH, et al. Recurrence of atrial fibrillation correlates with the extent of post-procedural late gadolinium enhancement: a pilot study. JACC Cardiovasc Imaging 2009;2(3):308–316.
17. Daccarett M, Badger TJ, Akoum N, et al. Association of left atrial fibrosis detected by

delayed-enhancement magnetic resonance imaging and the risk of stroke in patients with atrial fibrillation. J Am Coll Cardiol 2011;57(7):831–838.

18. Lustig M, Donoho DL, Pauly JM. Sparse MRI: the application of compressed sensing for rapid MR imaging. Magn Reson Med 2007;58(6):1182–1195.
19. Vasanawala SS, Alley MT, Hargreaves BA, Barth RA, Pauly JM, Lustig M. Improved pediatric MR imaging with compressed sensing. Radiology 2010;256(2):607–616.
20. Akçakaya M, Basha TA, Goddu B, et al. Low-dimensional-structure self-learning and thresholding: regularization beyond compressed sensing for MRI reconstruction. Magn Reson Med 2011;66(3):756–767.
21. Akçakaya M, Basha TA, Chan RH, et al. Accelerated contrast-enhanced whole-heart coronary MRI using low-dimensional-structure self-learning and thresholding. Magn Reson Med 2012;67(5):1434–1443.
22. Wang Y, Riederer SJ, Ehman RL. Respiratory motion of the heart: kinematics and the implications for the spatial resolution in coronary imaging. Magn Reson Med 1995;33(5):713–719.
23. Danias PG, Stuber M, Botnar RM, Kissinger KV, Edelman RR, Manning WJ. Relationship between motion of coronary arteries and diaphragm during free breathing: lessons from real-time MR imaging. AJR Am J Roentgenol 1999;172(4):1061–1065.
24. Kellman P, Arai AE, McVeigh ER, Aletras AH. Phase-sensitive inversion recovery for detecting myocardial infarction using gadolinium-delayed hyperenhancement. Magn Reson Med 2002;47(2):372–383.
25. Schmidt M, Nölker G, Marschang H, et al. Incidence of oesophageal wall injury post-pulmonary vein antrum isolation for treatment of patients with atrial fibrillation. Europace 2008;10(2):205–209.
26. Meng J, Peters DC, Hsing JM, et al. Late gadolinium enhancement of the esophagus is common on cardiac MR several months after pulmonary vein isolation: preliminary observations. Pacing Clin Electrophysiol 2010;33(6):661–666.
27. Tung P, Hong SN, Chan RH, et al. Abnormalities of the aorta are common following pulmonary vein isolation: a cardiac magnetic resonance imaging study. Circulation 2011;124(Suppl):A16972.
28. Sodickson DK, Manning WJ. Simultaneous acquisition of spatial harmonics (SMASH): fast imaging with radiofrequency coil arrays. Magn Reson Med 1997;38(4):591–603.
29. Pruessmann KP, Weiger M, Scheidegger MB, Boesiger P. SENSE: sensitivity encoding for fast MRI. Magn Reson Med 1999;42(5):952–962.
30. Griswold MA, Jakob PM, Heidemann RM, et al. Generalized autocalibrating partially parallel acquisitions (GRAPPA). Magn Reson Med 2002;47(6):1202–1210.
31. Pruessmann KP, Weiger M, Börnert P, Boesiger P. Advances in sensitivity encoding with arbitrary k-space trajectories. Magn Reson Med 2001;46(4):638–651.